J Neurophysiol 118: 344–352, 2017.
First published April 26, 2017; doi:10.1152/jn.00129.2017.

RESEARCH ARTICLE | *Higher Neural Functions and Behavior*

Entrainment of visual steady-state responses is modulated by global spatial statistics

Thomas Nguyen,[1] Karl Kuntzelman,[1] and Vladimir Miskovic[1,2]
[1]*Department of Psychology, State University of New York at Binghamton, Binghamton, New York; and* [2]*Center for Affective Science, State University of New York at Binghamton, Binghamton, New York*

Submitted 23 February 2017; accepted in final form 25 April 2017

Nguyen T, Kuntzelman K, Miskovic V. Entrainment of visual steady-state responses is modulated by global spatial statistics. *J Neurophysiol* 118: 344–352, 2017. First published April 26, 2017; doi:10.1152/jn.00129.2017.—The rhythmic delivery of visual stimuli evokes large-scale neuronal entrainment in the form of steady-state oscillatory field potentials. The spatiotemporal properties of stimulus drive appear to constrain the relative degrees of neuronal entrainment. Specific frequency ranges, for example, are uniquely suited for enhancing the strength of stimulus-driven brain oscillations. When it comes to the nature of the visual stimulus itself, studies have used a plethora of inputs ranging from spatially unstructured empty fields to simple contrast patterns (checkerboards, gratings, stripes) and complex arrays (human faces, houses, natural scenes). At present, little is known about how the global spatial statistics of the input stimulus influence entrainment of scalp-recorded electrophysiological signals. In this study, we used rhythmic entrainment source separation of scalp EEG to compare stimulus-driven phase alignment for distinct classes of visual inputs, including broadband spatial noise ensembles with varying second-order statistics, natural scenes, and narrowband sinewave gratings delivered at a constant flicker frequency. The relative magnitude of visual entrainment was modulated by the global properties of the driving stimulus. Entrainment was strongest for pseudonaturalistic broadband visual noise patterns in which luminance contrast is greatest at low spatial frequencies (a power spectrum slope characterized by $1/f^{-2}$).

NEW & NOTEWORTHY Rhythmically modulated visual stimuli entrain the activity of neuronal populations, but the effect of global stimulus statistics on this entrainment is unknown. We assessed entrainment evoked by *1*) visual noise ensembles with different spectral slopes, *2*) complex natural scenes, and *3*) narrowband sinusoidal gratings. Entrainment was most effective for broadband noise with naturalistic luminance contrast. This reveals some global properties shaping stimulus-driven brain oscillations in the human visual system.

entrainment; image amplitude; image statistics; spatial structure; steady-state visual evoked response

BRAIN RHYTHMS are ubiquitous over a number of different spatiotemporal scales with impressive conservation throughout the phylogenetic spectrum (Buzsáki et al. 2013). To gain further insight into their functions, investigators are increasingly turning to methods for selectively modulating frequency-delimited brain oscillations in experimental settings (Herrmann et al. 2016). Sensory stimuli can be used to drive brain oscillations by taking advantage of temporally periodic or quasi-periodic inputs (Keitel et al. 2017; Spaak et al. 2014). Rhythmic sensory stimulation evokes large-scale neuronal entrainment (known as steady-state responses) at multiple stages of the sensory processing hierarchy. For instance, periodic luminance modulation or pattern/contrast reversal elicits steady-state visual evoked potentials (SSVEPs) that can be recorded from the retina (Jacobs et al. 1996) and intracranial electrodes placed in the lateral geniculate nucleus and V1 (Krolak-Salmon et al. 2003; Rager and Singer 1998; Williams et al. 2004), as well as from surface electrodes covering parieto-occipital scalp regions (Herrmann 2001; Vialatte et al. 2010). Since their discovery by the early pioneers of neurophysiology (Adrian and Matthews 1934), visual steady-state responses have been widely used to examine research questions pertaining to low (Norcia et al. 2015; Regan 1989), mid (Alp et al. 2016; Gundlach and Müller 2013), and high levels of vision (Retter and Rossion 2016; Rossion 2014), as well as to probe the influence of attention (Keitel et al. 2014; Morgan et al. 1996; Müller and Hübner 2002), learning and memory (Keil et al. 2013; Koenig-Robert and VanRullen 2013; Martens et al. 2012; Moratti and Keil 2009) and affect (Wieser et al. 2016) on ongoing visual processes. A major advantage of SSVEPs over traditional visual evoked potentials is their high signal-to-noise ratio, enabling investigators to obtain a robust signal that requires fewer trials and is less susceptible to many common sources of recording artifacts (Vialatte et al. 2010).

Despite their widespread use, there are a number of unanswered questions about the spatiotemporal parameters that influence the SSVEP response. The possible existence of natural frequencies, specific rhythms for which the visuocortical system is preferentially tuned, remains a topic of debate. One perspective views the choice of stimulation frequency as largely arbitrary, a way of "wire-tapping" into the visual system without interfering with it (Keitel et al. 2014). In support of this hypothesis, there seem to be few constraints on the frequencies that are suitable for eliciting scalp-recorded SSVEPs; generally speaking, frequencies ranging anywhere from 1 to ~90 Hz are effective in driving the human visual cortex (Herrmann 2001). However, a number of existing reports indicate that particular stimulation frequencies are associated with more robust visual responses. Using empty full-field illumination, Herrmann (2001) found evidence for such

Address for reprint requests and other correspondence: V. Miskovic, Dept. of Psychology, SUNY Binghamton, Binghamton, NY 13902-6000 (e-mail: miskovic@binghamton.edu).

resonance phenomena at 10, 20, 40, and 80 Hz. Several other reports have indicated preferential responses when stimulation frequencies fall somewhere within the classical beta-band frequency range (14 to 16 Hz). Using EEG and positron emission tomography (PET) imaging with stroboscopic light modulated across a range of frequencies (5–40 Hz), 15-Hz stimulation was discovered to consistently produce the strongest occipital cortex activation (Pastor et al. 2003, 2007; but see Fawcett et al. 2004). Presentation of Gabor ellipsoids was subsequently found to elicit the strongest source level connectivity between visual cortex and extrastriate structures during stimulation delivered at the second harmonic of 15 Hz (Lithari et al. 2016). In a parallel line of research, 15-Hz intermittent photic stimulation exhibited the greatest likelihood of eliciting a photoparoxysmal response in patients with photosensitive epilepsy (Lopes da Silva and Harding 2011), and stroboscopic flicker in the 14- to 20-Hz range is associated with a peak in the formation of subjective visual patterns/geometric hallucinations among healthy populations (Remole 1971). There is convergent evidence, then, to suggest that 15-Hz flicker ought to elicit a strong entrainment of neuronal populations in the visual cortex.

Whereas a number of studies have examined the sensitivity of SSVEPs to different stimulation frequencies, considerably less is known about how altering the global spatial structure of a stimulus biases neuronal entrainment. A wide variety of stimuli have been used to drive visual brain oscillations, ranging from spatially unstructured light-emitting diodes (with varying colors), to simple checkerboard or sinusoidal grating patterns, to images of houses, human faces, bodies, and naturalistic scenes (Vialatte et al. 2010) with energy distribution across many spatial frequencies and orientations that activate numerous cell populations in calcarine cortex (Martens et al. 2011). Across a range of situations, the choice of stimulus is known to shape the electrophysiological signature of visual responses. For example, intracranial recordings from human V1/V2/V3 have recently (Hermes et al. 2015) demonstrated that visually evoked narrowband gamma oscillations are stimulus-dependent, being observed for some classes of spatial contrast patterns (gratings) but not others (noise patches and natural images). Similarly, in feline visual cortex, both local field potential and multiunit recordings have revealed distinct types of activity patterns in V1 for drifting sinusoidal gratings compared with natural images and pseudo-naturalistic visual noise with modified spatiotemporal content (Kayser et al. 2003). Our goal was primarily to extend the exploration of visual steady-state responses to spatially broadband stimuli.

Numerous lines of evidence suggest that the visual system is phylogenetically and ontogenetically adapted to the statistics of natural environments (Geisler 2008; Párraga et al. 2000) and that regularities of sensory stimuli are extracted even at the earliest levels of the visual processing stream (De Cesarei et al. 2017; Simoncelli and Olshausen 2001). Although researchers have mostly relied on mathematically elegant basis sets (e.g., Gabors) for measuring visual responses, these narrowband stimuli have little ecological relevance (Felsen and Dan 2005; Olshausen and Field 2005), and there is concern that they will not be sufficient to develop a complete understanding of human visual function (e.g., Felsen and Dan 2005).

A principled way of controlling the second-order statistics of complex (broadband) visual stimuli is by generating synthetic spatial noise ensembles with random phase but distinct distributions of spectral power (denoted as different colors of noise). Common variants of visual noise patterns are referred to as white, pink, and Brownian noise. When plotted on a log-log scale, the power spectral drop-off of each type of colored noise can be fit by a $1/f^{\beta}$ function, with different β exponents corresponding to varied colors of noise. White noise contains equal energy across spatial frequencies, is uncorrelated, and has a flat power spectrum ($1/f^{0}$), whereas pink ($1/f^{-1}$) and Brownian noise ($1/f^{-2}$) exhibit correlations with more energy concentration at lower frequencies. Natural visual environments exhibit orientation-averaged spectral power slopes around $1/f^{-2}$ (Billock 2000; Simoncelli and Olshausen 2001; Tolhurst et al. 1992; Torralba and Oliva 2003), reflecting a preponderance of gradual luminance transitions. Visual noise with $1/f^{-2}$ power spectra can therefore be considered pseudo-naturalistic (naturalistic in terms of the power but not phase components) and psychophysical sensitivity is indeed enhanced for such noise patterns (Baker et al. 2009; Knill et al. 1990; Tadmor and Tolhurst 1994).

In the present study, we examined the strength of neuronal entrainment during periodic drive as a function of the global spatial properties of the visual input while the temporal luminance modulation function was a square wave with a frequency of 15 Hz. Specifically, we flickered a number of exemplars of each type of broadband visual colored noise (white, pink, and Brownian) while measuring stimulus-driven phase alignment in high-density EEG. In addition to the synthetically constructed spatial noise ensembles, we included natural scenes and narrowband sine-wave gratings, two categories of stimuli that have been commonly used in prior research. Given that the visual system appears to be tuned for a specific range of second-order luminance statistics (e.g.,$1/f^{-2}$ power spectra), we expected to find stimulus-dependent shifts in the magnitude of population-level neuronal entrainment. To obtain a more precise isolation of the sensory entrained response from ongoing brain activity and to overcome a limitation of conventional SSVEP analyses (individual variance in the scalp projection of SSVEPs), we used a multivariate source separation procedure known as rhythmic entrainment source separation (RESS) (Cohen and Gulbinaite 2017). This approach allowed us to extract a single, weighted component time series signal and permitted a comparison with the conventional SSVEP analysis.

MATERIALS AND METHODS

Participants

A total of 16 participants from SUNY Binghamton completed the experiment. The group was made up of 10 women and 6 men, ranging in age from 18 to 33 yr (mean age 21.3 yr, SD 2.7 yr). Participants were tested for 20/20 or corrected-to-20/20 vision using a Snellen eye chart. Two participants were excluded from analysis due to excessively noisy EEG recordings and the absence of apparent EEG entrainment to the flicker frequency, resulting in a total of 14 participants for the final analyses. All of the experimental procedures were approved by the institutional ethics review board.

Materials and Procedure

Stimuli. Five different image categories were used in this experiment: white noise, pink noise, Brownian noise, natural scenes, and

sine-wave gratings. The broadband spatial noise ensembles were generated as two-dimensional matrices in MATLAB using independent simulation runs. The visual noise ensembles all contained random phase coefficients drawn from a uniform distribution between 0 and 2π. The slope of the spatial frequency power spectrum for each exemplar of a noise class was set according to its color. The natural images were randomly selected from the van Hateren Natural Scene Database (van Hateren and van der Schaaf 1998). The scenes depicted a mixture of natural (e.g., trees, clouds, landscapes) and manmade settings (e.g., buildings). For each of the broadband image exemplars, we plotted its corresponding one-dimensional radially averaged power spectrum on a log-log plot and estimated the β exponent as the slope of the first-degree polynomial fit (see summary of mean slopes in Fig. 1). The spatial frequency of the sine-wave gratings (2.7 cycles/°) was kept constant, but orientation varied in 9° steps, ranging from 0 to 360°.

Each image category had 40 unique exemplars, and none of the images were repeated in the course of the experiment. All of the images were converted to grayscale and equated in their mean luminance (measured as 16.5 cd/m^2 on the monitor display). The mean Michelson contrast, calculated as $[(I_{max} - I_{min})/(I_{max} + I_{min})] \times 100$, was 57%. All stimuli subtended a horizontal visual angle of 9.4° and a vertical visual angle of 6.4°.

Procedure. After providing written informed consent and initial screening to rule out photic epilepsy, participants were seated in a dimly lit experimental room in which a 129-sensor EEG net was applied. Participants were seated 1.15 m from the display and instructed to view the images attentively while minimizing eye movements and blinks. Images were presented in the center of the display against a uniform gray background (40 cd/m^2) on a 23.6-in. ASUS LCD monitor with 1-ms response time and 60-Hz refresh rate. The order of image presentation was randomized separately for each individual. The images were flickered ON/OFF for 4 s at a rate of 15 Hz (60 full cycles within a trial) using a 50% active duty cycle. The intertrial interval consisted of a central fixation cross, presented for a random duration between 2 and 3 s. A white noise machine provided an auditory screen.

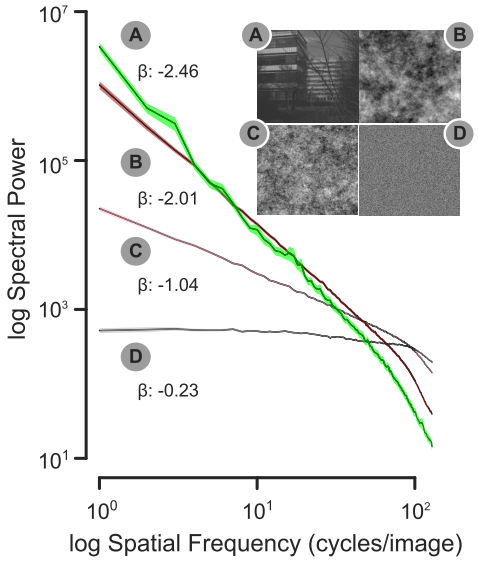

Fig. 1. Mean, orientation-averaged (1-dimensional) power spectrum for natural scenes (*A*) and each of the colored spatial noise ensembles (*B*, Brownian noise; *C*, pink noise; *D*, white noise), along with the mean slope (β) of the spectral power drop-off. Note that the slopes for the grating stimuli are not provided, because these estimates are heavily influenced by the large peaks that characterize narrowband sine gratings. Shading indicates SE.

EEG Data Acquisition and Processing

EEG was continuously recorded from 129 sensors using an Electrical Geodesics HydroCel Geodesic Sensor Net, digitized at a rate of 1 kHz using the vertex sensor (Cz) as the recording reference, with the online bandpass filter set at 100 Hz (low pass). Sensor impedances were kept below 60 kΩ.

Offline EEG processing was implemented using the Electro MagnetoEncephalography software (EMEGS) toolbox for MATLAB (Peyk et al. 2011) and in-house custom-written MATLAB routines. Epochs were segmented to contain 600 ms of activity before stimulus onset and 5 s after stimulus onset (these times include 1-s poststimulus offset). The data were then filtered using a 50-Hz (45 dB/octave, 14th-order Butterworth) low pass and an 0.8-Hz (20 dB/octave, 2nd-order Butterworth) high pass. Statistical parameters were used to find and remove artifact-contaminated channels and trials by means of the SCADS automated procedure (Junghöfer et al. 2000). The original recording reference (Cz) was first used to detect recording artifacts, and then the data were average referenced to detect global artifacts. Subsequently, bad sensors within individual trials were identified and interpolated on the basis of rejection criteria for the mean absolute (rectified) amplitude, the variability over time points, and the maximum first-order derivate (gradient). Trials were rejected when more than 20 sensors of 129 were identified as outliers using the statistical criteria mentioned previously. Using this method, we retained 78% of trials, with no difference in the number of artifact-free trials as a function of stimulus category ($F < 1$).

Rhythmic Entrainment Source Separation Procedure

All artifact-free/artifact-corrected electrode data from each participant were submitted to the RESS procedure, which is described in detail elsewhere (see Cohen and Gulbinaite 2017 for accompanying MATLAB code). Briefly, the steps involved were as follows: *1*) $N \times N$ covariance matrices were constructed using electrode data that were narrow bandpass filtered [0.5-Hz full width at half-maximum (FWHM) Gaussian] at the driving frequency (S covariance matrix) and at neighboring (±1 Hz from driving frequency, 1-Hz FWHM Gaussian filter) frequencies (R covariance matrices). The face and neck electrodes were removed before this step to minimize the contribution of noisy channels. *2*) Next, a generalized eigendecomposition was performed to isolate the eigenvectors that separated the S from the average of the two R covariance matrices. *3*) Finally, the eigenvector with the largest eigenvalue was used to construct a spatial filter, which involves multiplication of the eigenvector with the electrode data to produce a single, weighted time series (the RESS component) that can be analyzed by means of the traditional time × frequency methods used for sensor-space data. The same three steps were performed for neighboring frequencies above and below the stimulation frequency, and the resulting spectra were used to normalize the coefficients associated with the analysis based on the frequency of interest, which yields a signal-to-noise ratio (SNR) insensitive to the typical 1/*f* slope of human EEG. Figure 2 illustrates the grand-averaged RESS time series signal, along with its topographic distribution (as illustrated in Fig. 2 *insets*, we found no appreciable topographic differences across the 5 different stimulus categories and therefore do not report these any further). Comparison of the SNR between the 15-Hz RESS (mean SNR = 60) and the conventional SSVEP estimate (mean SNR = 18.5) at electrode Oz (see Fig. 2) illustrates the advantage of the RESS method in extracting the stimulus-driven oscillatory brain response. Identical procedures were used to reconstruct the RESS at the driving frequency ($1f$) as well as the second harmonic component at 30 Hz ($2f$), given the clear presence of a frequency-doubled response in the majority of subjects, as reported in previous studies (Heinrichs-Graham and Wilson 2012). We did not focus on the third harmonic because it was small in magnitude and inconsistently expressed across individual subjects.

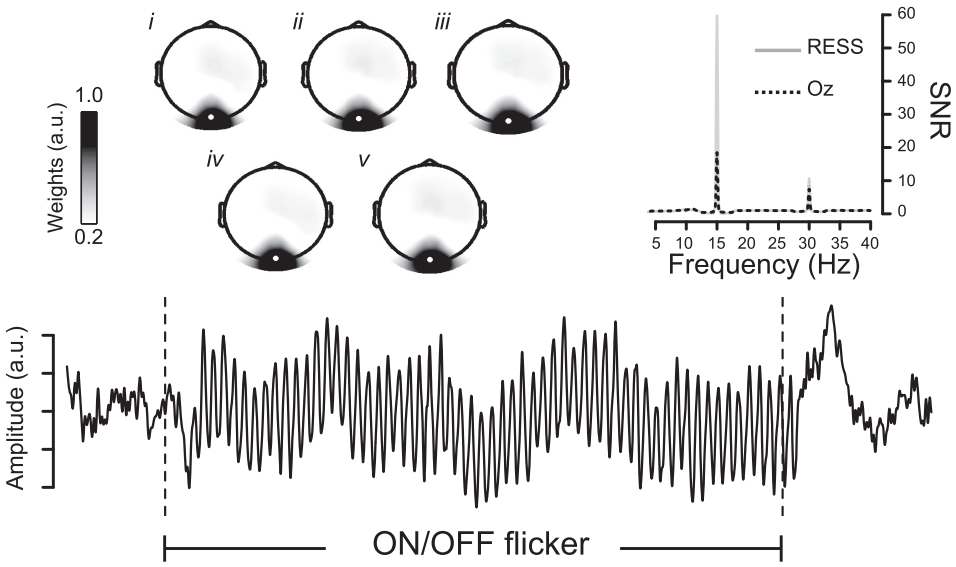

Fig. 2. A multivariate source separation method, rhythmic entrainment source separation (RESS), was used to isolate the stimulus-driven component of brain electrical activity as a single time series. The 15-Hz RESS component is depicted in the time domain (averaged over all trials and subjects). A comparison of the SNR spectrum between the RESS and the classical SSVEP response at the Oz electrode is depicted in the *inset* at *top right*. Topographic weights of the 15-Hz RESS component (with Oz electrode highlighted) are shown for each of Brownian (*i*), pink (*ii*), and white (*iii*) broadband visual noise patterns, as well as for natural scenes (*iv*) and sine-wave gratings (*v*). a.u., Arbitrary units.

In light of the evidence that SSVEPs are better explained as the result of phase alignment driven by the rhythmicity of the sensory train rather than as the result of single trial amplitude modulations (Moratti et al. 2007), we elected to quantify intertrial phase clustering as the most direct index of ongoing neuronal entrainment.[1] Accordingly, a complex 7-cycle Morlet wavelet with a center frequency of 15 Hz (wavelet FWHM of 5 Hz) was convolved with the single-trial RESS components for each of the 5 stimulus conditions. A 14-cycle Morlet wavelet with a center frequency of 30 Hz was used for the second harmonic analyses, to keep the FWHM constant. Intertrial phase clustering (ITPC) was then calculated for both the driving frequency and the second harmonic as the average of the unit-length phase vectors over trials for each time and frequency point. The ITPC index is bounded between 0 (uniform phase angle distribution over trials) and 1 (phase angles that are perfectly aligned trial by trial).

[1] In all major respects, our findings were nearly identical when the SNR of trial-averaged spectral amplitude was used as the dependent variable instead of intertrial phase clustering.

RESULTS

Electrode-Level SSVEP Entrainment

The magnitude of rhythmic entrainment was modulated by the global structure of the visual stimulus, as illustrated in Fig. 3. This impression was confirmed by an effect of stimulus category on the $1f$ ITPC index averaged over the time interval from 600 until 4,000 ms poststimulus onset at electrode Oz [$F(4,52) = 5.20$, $P = 0.001$, partial $\eta^2 = 0.29$]. We first consider the broadband visual noise patterns with distinct spectral drop-offs. A general observation from our data is that the spatially correlated sequences (Brownian and pink) evoked stronger entrainment than spatially uncorrelated pixel noise with a flat power spectrum. Visual noise ensembles with naturalistic amplitude spectra ($1/f^{-2}$) were associated with the largest overall $1f$ entrainment (refer to Table 1 for the results of pairwise contrasts).

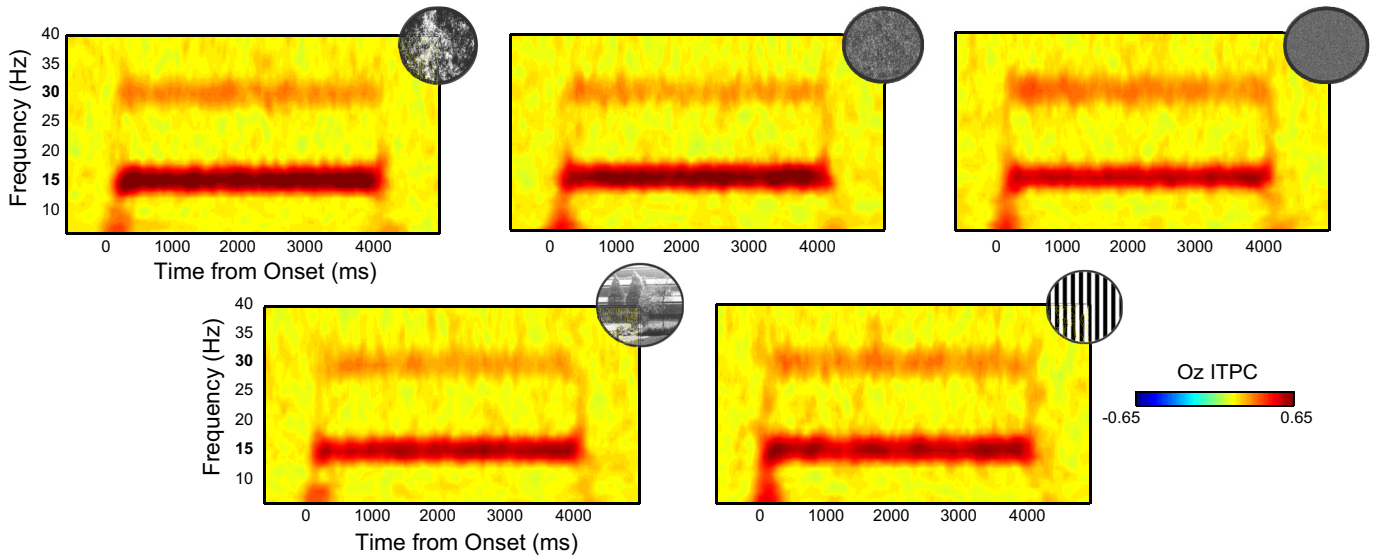

Fig. 3. Intertrial phase coherence (ITPC) time courses at electrode Oz for the visual noise ensembles (*top* row; Brownian, pink, and white noise from *left* to *right*) as well as the natural scenes and sine-wave gratings (*bottom* row). Bold numbers on the frequency axis highlight frequency-following ($1f$: 15 Hz) and frequency-doubled ($2f$: 30 Hz) EEG responses.

Table 1. *Probability values (FDR corrected) and effect sizes for 15-Hz Oz ITPC pairwise contrasts*

Contrast	*P*	Cohen's d_z
Brownian vs. white noise	**0.04**	0.89
Brownian vs. pink noise	0.63	0.14
Pink vs. white noise	**0.04**	0.78
Brownian noise vs. natural scenes	**0.01**	1.13
Brownian noise vs. gratings	**0.04**	0.74
Pink noise vs. natural scenes	**0.04**	0.78
Pink noise vs. gratings	0.27	0.40
White noise vs. natural scenes	0.63	0.17
Natural scenes vs. gratings	0.63	0.13

Contrast values with $P < 0.05$ are in bold type.

The artificially generated, pseudo-naturalistic visual noise patterns also elicited greater electrode-level entrainment responses compared with actual natural scenes and narrowband sine-wave gratings. There was no reliable effect of stimulus category on the magnitude of $2f$ entrainment ($F < 1$).

Two key limitations of conventional, electrode-level SSVEP analyses are that they may not be optimal for separating entrained neuronal activity from ongoing, endogenous brain oscillations and that there is substantial individual variability in the topographic distribution of extracranially recorded brain potentials. The latter issue is illustrated by inspecting the scalp distributions of SSVEP ITPCs shown in Fig. 4. To address these limitations, we next turned to using the rhythmic entrainment source separation technique (see Fig. 2).

Source-Separated RESS Entrainment

Figure 5 depicts the stimulus-dependent ITPC modulation curves for the $1f$ RESS signal component. Since the time varying fluctuations were negligible, the ITPC index was averaged over time as above and entered into a repeated-measures ANOVA using the within-subjects factor of stimulus category. This analysis revealed a significant main effect [$F(4,52) = 7.32$, $P < 0.001$, partial $\eta^2 = 0.36$] that was followed up with a series of post hoc pairwise contrasts (summarized in Table 2).

The results of the RESS analysis confirmed that the Brownian ($1/f^{-2}$) spatial arrangement evoked the largest magnitude of entrainment (mean ITPC 0.79, SE 0.04) and the white noise sequence the weakest (mean ITPC 0.69, SE 0.04), with the pink noise ensemble (mean ITPC 0.75, SE 0.04) intermediate between them. This pattern was consistent across individuals as evidenced by the single-subject difference plots illustrated in Fig. 6. The broadband pseudo-naturalistic, Brownian, and pink noise visual patterns evoked greater magnitude of phase alignment than either the natural scenes or the sine-wave gratings.

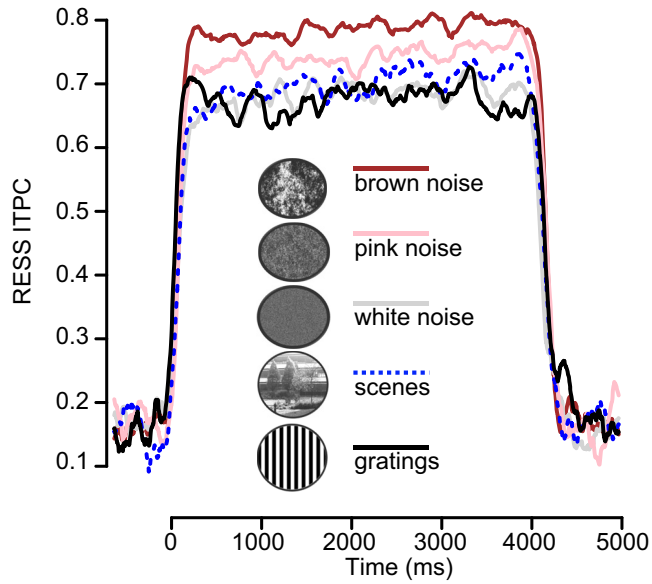

Fig. 5. Mean 15-Hz RESS ITPC, shown separately for each of the 5 stimulus categories. The stimulus flicker period started at 0 ms and ended at 4,000 ms.

Overall, phase alignment for the second harmonic component of the RESS was considerably weaker ($2f$ mean ITPC 0.42, SE 0.03) compared with that of the driving frequency ($1f$ mean ITPC 0.72, SE 0.04). Contrary to a previous report noting that only a minority of individuals exhibit peak entrainment at the driving frequency of a spatially homogenous field (Heinrichs-Graham and Wilson 2012), only 14% of our sample exhibited stronger entrainment at the second harmonic, and this was observed only when the driving stimulus consisted of white noise or sine-wave gratings. There was a positive correlation of ITPC values for the first and second harmonic RESS components (Spearman's $\rho = 0.62$), suggesting some shared variance.

There was a relatively weak effect of stimulus category on the second harmonic RESS component [$F(4,52) = 2.65$, $P = 0.05$, partial $\eta^2 = 0.02$]. This reflected the finding that pink pixel noise evoked less second-harmonic phase alignment than either white [$t(13) = 2.40$, $P = 0.03$, Cohen's $d_z = 0.67$] or Brownian noise [$t(13) = 2.59$, $P = 0.02$, Cohen's $d_z = 0.72$].

DISCUSSION

We investigated the magnitude of population-level rhythmic entrainment for narrowband and broadband visual ensembles

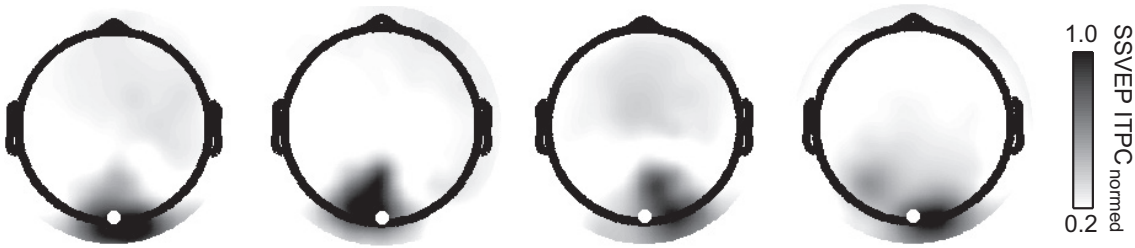

Fig. 4. Raw SSVEP ITPC topographies illustrating individual variance in $1f$ spatial distribution around the Oz target electrode (highlighted as a white circle). The subject at *left* shows a distribution that is concentrated and symmetric around the target electrode. The next 2 subjects exhibit topographic shifts to the left and right of Oz, respectively, whereas the subject at *right* exhibits an asymmetric (left parietal to right occipital) distribution. Each subject's SSVEP ITPC has been normalized to their individual maximum value.

Table 2. *Probability values (FDR corrected) and effect sizes for 15-Hz RESS ITPC pairwise contrasts*

Contrast	*P*	Cohen's d_z
Brownian vs. white noise	**0.03**	0.85
Brownian vs. pink noise	**0.04**	0.75
Pink vs. white noise	0.09	0.52
Brownian vs. natural scenes	**0.007**	1.12
Brownian vs. gratings	**0.002**	1.40
Pink vs. natural scenes	0.07	0.62
Pink vs. gratings	**0.04**	0.72
White vs. natural scenes	0.47	0.22
Natural scenes vs. gratings	0.09	0.53

Contrast values with $P < 0.05$ are in bold type.

with different global structures. To gain better control over the second-order statistics of our broadband stimuli, we generated synthetic spatial noise patterns with distinct power slope exponents. We then applied a multivariate source separation technique to effectively extract human brain oscillatory responses to the flickering visual stimuli. Although all visual stimulus categories evoked robust neural entrainment, the relative magnitude of stimulus-driven phase coherence varied as a function of global second-order spatial statistics. In short, we discovered strongest entrainment of the visual steady-state response for Brownian spatial noise (a $1/f^{-2}$ spectral power drop-off), followed by pink noise. The flat power spectrum of white noise ensembles emerged as the least effective of the visual noise patterns.

Rhythmic Entrainment for Periodically Modulated Broadband Visual Stimuli

Our findings demonstrate that spatially broadband noise patterns with naturalistic amplitude structure (i.e., more luminance contrast at lower, relative to higher, spatial frequencies) evoke stronger 1*f* visual steady-state responses. Scalp-recorded brain oscillations evoked by periodic stimulus drive, therefore, seem to be relatively dominated by neuronal populations that are tuned for lower spatial frequency content (see Miskovic et al. 2015, using band-passed achromatic and chromatic natural scenes). Retinotopic mapping of human visual cortex using functional magnetic resonance imaging (fMRI) has demonstrated the existence of smooth variation in band-pass tuning throughout early visual cortex (Henriksson et al. 2008), with progressively more low-pass tuning in areas V2 through V5 (Singh et al. 2000). Scalp-recorded visual steady-state responses are likely to include some weighted combination of activity emanating from multiple extrastriate regions (Vialatte et al. 2010).

It is tempting to infer on the basis of these findings that neuronal entrainment is enhanced for stimuli that more closely match the types of second-order luminance statistics for which our visual systems are adapted and for which human observers are known to exhibit improved perceptual discrimination (Baker et al. 2009; Knill et al. 1990; Tadmor and Tolhurst 1994). However, this straightforward interpretation is complicated by our observation that flickering natural scenes produced less entrainment than the synthetic, Brownian noise patches. There are several potential explanations for this apparently contradictory finding.

First, compared with synthetic visual noise, the exemplars used in our natural scene category constituted a more heterogenous sample of stimuli, including images with predominant low spatial frequency content (clouds, foggy pastoral settings) and others with more high spatial frequency content (tree branches with dense foliage). Moreover, these scenes differed in the amount of structural complexity (i.e., the number of edges/lines). In previous work that has focused on the early (P1 and N1) visual event-related potentials (ERPs), increasing the steepness of spectral amplitude slopes exerted a monotonic enhancement of P1 magnitude for visual noise patterns and simple natural scenery with few edges (Hansen et al. 2011, 2012). However, this relationship between luminance contrasts and ERP amplitudes was no longer observed for natural scenes that were high in structural complexity. The large variance of exemplars contained in our natural scene category might thereby have been partly responsible for reducing the degree of intertrial EEG phase alignment. By comparison, noise patterns do not contain broadband edges.

Second, natural images possess pronounced orientation anisotropies, with more luminance contrast at cardinal relative to oblique orientations (Hansen and Essock 2004). As is evident from the two-dimensional spectral contour plots depicted in Fig. 7, visual noise patterns are isotropic in their Fourier power, despite the similarities of $1/f^{-2}$ noise and natural scenes in terms of their orientation averaged spectra. Orientation anisotropy may influence the visual steady-state response in unpredictable ways especially in light of evidence that human observers are differentially sensitive to cardinal vs. oblique luminance contrasts in broadband stimuli (Essock et al. 2003).

Finally, it deserves to be emphasized that despite any similarities in the second-order statistics of $1/f^{-2}$ visual noise patterns and natural scenes, these categories possessed very different higher order statistics carried in their phase spectra. Previous recordings from cat V1 have demonstrated that these cells are relatively insensitive to higher order statistics (Kayser et al. 2003). However, sensitivity to phase structure is found at virtually all levels of the human visual system, including V1 (Felsen et al. 2005; Henriksson et al. 2009; Perna et al. 2008), and higher order statistics almost certainly influence scalp-recorded visual steady-state responses.

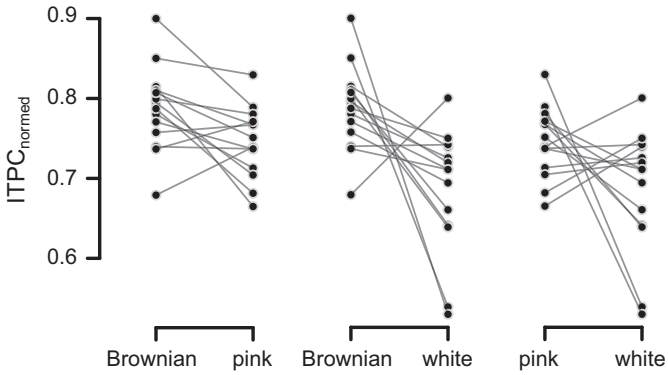

Fig. 6. Single-subject data depicting visual noise-dependent differences in 15-Hz RESS ITPC, normalized to remove between-subject variability of ITPC values following the method described in Morey (2008). The normalization procedure was performed for illustrative purposes only.

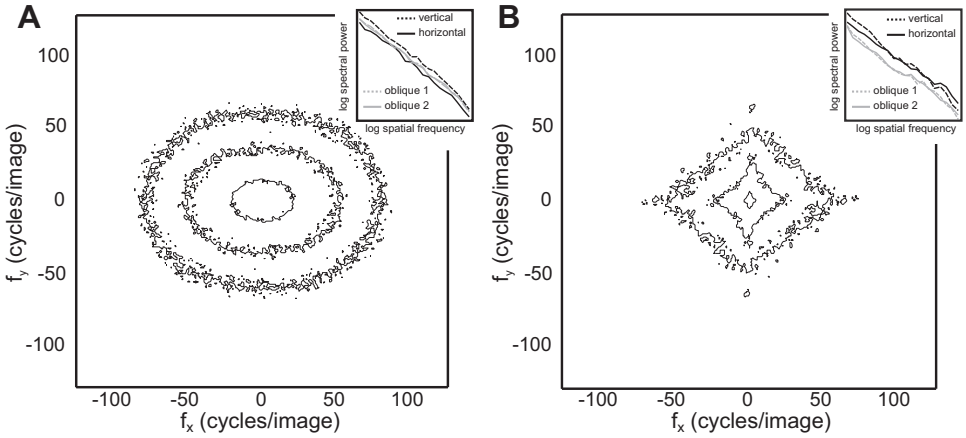

Fig. 7. Spectral contour plots for the averaged Brownian noise ensembles (*A*) and natural scenes (*B*), arranged such that the inner contour represents 60% and the outer contours 80% and 90%, respectively, of image energy. Insets (*top right*) depict 1-dimensional power spectra for 4 orientation bins. Note that the visual noise patterns are orientationally isotropic and do not display the biases in Fourier power for cardinal relative to oblique axes that are evident in natural scenes.

Methodological Considerations

Our main findings at the driving frequency (1*f*) were observed using both the conventional, target electrode approach for quantifying SSVEPs and the RESS method. However, the latter allowed us to avoid using a common target electrode that may not correspond to the optimal SNR for any given individual. We noted consistently higher SNR values for the RESS compared with the traditional approach and a greater effect size in the omnibus analysis.

In addition to entrainment at 1*f*, when employing the RESS method we observed substantial second harmonic (2*f*) entrainment. In agreement with previous reports (Heinrichs-Graham and Wilson 2012), we interpret this to be a physiological nonlinearity introduced by the visual system given that the spectral decomposition of a square wave with a 50% active duty yields only odd harmonics. Neural responses at twice the input frequency of stimulation likely emerge as the result of full-wave rectification processes in the visual hierarchy (Shapley 2009) and are observed in single units (De Valois et al. 1982; Jagadeesh et al. 1997) as well as at the aggregate population level. These responses are believed to emerge from partially independent neuronal populations (Kim et al. 2011; Pastor et al. 2003, 2007), a suggestion that is consistent with our observation that the second harmonic component was influenced by the global structure of visual noise in a distinct way from the frequency-following entrainment.

Limitations in Experimental Design

It is possible that some of our findings were specific to stimulation frequency. For instance, spatial frequency tuning curves for narrowband sinusoidal luminance patterns vary as a function of reversal rate, a finding that was interpreted to reflect distinct resonant features of specific retinostriate connections (Tyler et al. 1978). More recently, distinct temporal tuning profiles have been reported for human faces compared with words (Yeatman and Norcia 2016). Functional neuroimaging suggests that there may exist a gradient of optimal stimulation frequencies, with peak frequency descending, as one progresses along the ventral visual stream, from primary visual cortex to the more object-selective inferotemporal cortex (McKeeff et al. 2007). On the basis of these findings, our choice of stimulation frequency would have favored a response predominantly driven by V1 neuronal populations, a suggestion that seems generally consistent with the posterior occipital topographic distribution of the RESS component.

The possible role that attention might have played in the current investigation cannot be discounted. We used a free-viewing task during which participants were encouraged to remain attentive throughout the course of the experimental procedure. It is highly likely that participants naturally attended to the various stimulus categories to different degrees. For example, despite their random phase structure, Brownian spatial noise ensembles typically have a cloud- or fog-like appearance that might be perceived as inherently more interesting compared with the dead TV channel appearance of white noise. Because attention is known to enhance the phase synchronization of SSVEPs (Kim et al. 2007), semantic structure may have inadvertently contributed to our findings. However, these cognitive factors are likely to be in operation for most, if not all, studies that have examined the influence of factors such as spatial frequency (De Cesarei et al. 2013) and amplitude/phase scrambling (Bieniek et al. 2012) on visual brain potentials in light of the impact that these manipulations have on the observer's ability to successfully extract scene gist. Although it seems unlikely that this is a complete explanation of our results given the relatively weaker entrainment to natural scenes compared with pseudo-naturalistic broadband noise, use of a concurrent, attention demanding task may be a worthwhile step to alleviate this concern in the future.

Future Directions

Given the high SNR of the RESS component and its ability to track single-trial phase/amplitude dynamics (Cohen and Gulbinaite 2017), it will be productive in the future to focus on modeling responses to individual scenes. One approach might be to construct multivariate regression models predicting the electrocortical response on the basis of scene statistics from a collection of natural images. We note that in this work we manipulated the global characteristics of visual stimuli and then ascertained their impact on rhythmic phase alignment. The visual system presumably engages in local sampling, and although there is nontrivial variance in receptive field sizes of the V1 neurons known to be directly sensitive to spatial frequency, even the most generous fMRI-based estimates of ~2–3° visual angle (Fracasso et al. 2016) are substantially smaller than the stimuli used here. Consequently, quantification of local image features might be particularly informative.

Another productive avenue for research might involve replicating findings both in vivo and in silico by extending the extant corticothalamic neural field models of rhythmic drive (Roberts and Robinson 2012) for broadband spatial structures.

GRANTS

This work was partially supported by National Institute of Mental Health Grant R03 MH105716 (to V. Miskovic).

DISCLOSURES

No conflicts of interest, financial or otherwise, are declared by the authors.

AUTHOR CONTRIBUTIONS

T.N. and V.M. conceived and designed research; T.N. performed experiments; T.N. and V.M. analyzed data; T.N., K.K., and V.M. interpreted results of experiments; V.M. prepared figures; T.N., K.K., and V.M. drafted manuscript; T.N., K.K., and V.M. edited and revised manuscript; T.N., K.K., and V.M. approved final version of manuscript.

REFERENCES

Adrian ED, Matthews BH. The Berger rhythm: potential changes from the occipital lobes in man. *Brain* 57: 355–385, 1934. doi:10.1093/brain/57.4.355.

Alp N, Kogo N, Van Belle G, Wagemans J, Rossion B. Frequency tagging yields an objective neural signature of Gestalt formation. *Brain Cogn* 104: 15–24, 2016. doi:10.1016/j.bandc.2016.01.008.

Baker DH, Graf EW. Natural images dominate in binocular rivalry. *Proc Natl Acad Sci USA* 106: 5436–5441, 2009. doi:10.1073/pnas.0812860106.

Bieniek MM, Pernet CR, Rousselet GA. Early ERPs to faces and objects are driven by phase, not amplitude spectrum information: evidence from parametric, test-retest, single-subject analyses. *J Vis* 12: 1–24, 2012. doi:10.1167/12.13.12.

Billock VA. Neural acclimation to 1/f spatial frequency spectra in natural images transduced by the human visual system. *Physica D* 137: 379–391, 2000. doi:10.1016/S0167-2789(99)00197-9.

Buzsáki G, Logothetis N, Singer W. Scaling brain size, keeping timing: evolutionary preservation of brain rhythms. *Neuron* 80: 751–764, 2013. doi:10.1016/j.neuron.2013.10.002.

Cohen MX, Gulbinaite R. Rhythmic entrainment source separation: optimizing analyses of neural responses to rhythmic sensory stimulation. *Neuroimage* 147: 43–56, 2017. doi:10.1016/j.neuroimage.2016.11.036.

De Cesarei A, Loftus GR, Mastria S, Codispoti M. Understanding natural scenes: Contributions of image statistics. *Neurosci Biobehav Rev* 74: 44–57, 2017. doi:10.1016/j.neubiorev.2017.01.012.

De Cesarei A, Mastria S, Codispoti M. Early spatial frequency processing of natural images: an ERP study. *PLoS One* 8: e65103, 2013. doi:10.1371/journal.pone.0065103.

De Valois RL, Albrecht DG, Thorell LG. Spatial frequency selectivity of cells in macaque visual cortex. *Vision Res* 22: 545–559, 1982. doi:10.1016/0042-6989(82)90113-4.

Essock EA, DeFord JK, Hansen BC, Sinai MJ. Oblique stimuli are seen best (not worst!) in naturalistic broad-band stimuli: a horizontal effect. *Vision Res* 43: 1329–1335, 2003. doi:10.1016/S0042-6989(03)00142-1.

Fawcett IP, Barnes GR, Hillebrand A, Singh KD. The temporal frequency tuning of human visual cortex investigated using synthetic aperture magnetometry. *Neuroimage* 21: 1542–1553, 2004. doi:10.1016/j.neuroimage.2003.10.045.

Felsen G, Dan Y. A natural approach to studying vision. *Nat Neurosci* 8: 1643–1646, 2005. doi:10.1038/nn1608.

Felsen G, Touryan J, Han F, Dan Y. Cortical sensitivity to visual features in natural scenes. *PLoS Biol* 3: e342, 2005. doi:10.1371/journal.pbio.0030342.

Fracasso A, Petridou N, Dumoulin SO. Systematic variation of population receptive field properties across cortical depth in human visual cortex. *Neuroimage* 139: 427–438, 2016. doi:10.1016/j.neuroimage.2016.06.048.

Geisler WS. Visual perception and the statistical properties of natural scenes. *Annu Rev Psychol* 59: 167–192, 2008. doi:10.1146/annurev.psych.58.110405.085632.

Gundlach C, Müller MM. Perception of illusory contours forms intermodulation responses of steady state visual evoked potentials as a neural signature of spatial integration. *Biol Psychol* 94: 55–60, 2013. doi:10.1016/j.biopsycho.2013.04.014.

Hansen BC, Essock EA. A horizontal bias in human visual processing of orientation and its correspondence to the structural components of natural scenes. *J Vis* 4: 1044–1060, 2004. doi:10.1167/4.12.5.

Hansen BC, Jacques T, Johnson AP, Ellemberg D. From spatial frequency contrast to edge preponderance: the differential modulation of early visual evoked potentials by natural scene stimuli. *Vis Neurosci* 28: 221–237, 2011. doi:10.1017/S095252381100006X.

Hansen BC, Johnson AP, Ellemberg D. Different spatial frequency bands selectively signal for natural image statistics in the early visual system. *J Neurophysiol* 108: 2160–2172, 2012. doi:10.1152/jn.00288.2012.

Heinrichs-Graham E, Wilson TW. Presence of strong harmonics during visual entrainment: a magnetoencephalography study. *Biol Psychol* 91: 59–64, 2012. doi:10.1016/j.biopsycho.2012.04.008.

Henriksson L, Hyvärinen A, Vanni S. Representation of cross-frequency spatial phase relationships in human visual cortex. *J Neurosci* 29: 14342–14351, 2009. doi:10.1523/JNEUROSCI.3136-09.2009.

Henriksson L, Nurminen L, Hyvärinen A, Vanni S. Spatial frequency tuning in human retinotopic visual areas. *J Vis* 8: 1–13, 2008. doi:10.1167/8.10.5.

Hermes D, Miller KJ, Wandell BA, Winawer J. Stimulus dependence of gamma oscillations in human visual cortex. *Cereb Cortex* 25: 2951–2959, 2015. doi:10.1093/cercor/bhu091.

Herrmann CS. Human EEG responses to 1-100 Hz flicker: resonance phenomena in visual cortex and their potential correlation to cognitive phenomena. *Exp Brain Res* 137: 346–353, 2001. doi:10.1007/s002210100682.

Herrmann CS, Murray MM, Ionta S, Hutt A, Lefebvre J. Shaping intrinsic neural oscillations with periodic stimulation. *J Neurosci* 36: 5328–5337, 2016. doi:10.1523/JNEUROSCI.0236-16.2016.

Jacobs GH, Neitz J, Krogh K. Electroretinogram flicker photometry and its applications. *J Opt Soc Am A Opt Image Sci Vis* 13: 641–648, 1996. doi:10.1364/JOSAA.13.000641.

Jagadeesh B, Wheat HS, Kontsevich LL, Tyler CW, Ferster D. Direction selectivity of synaptic potentials in simple cells of the cat visual cortex. *J Neurophysiol* 78: 2772–2789, 1997.

Junghöfer M, Elbert T, Tucker DM, Rockstroh B. Statistical control of artifacts in dense array EEG/MEG studies. *Psychophysiology* 37: 523–532, 2000. doi:10.1111/1469-8986.3740523.

Kayser C, Salazar RF, Konig P. Responses to natural scenes in cat V1. *J Neurophysiol* 90: 1910–1920, 2003. doi:10.1152/jn.00195.2003.

Keil A, Miskovic V, Gray MJ, Martinovic J. Luminance, but not chromatic visual pathways, mediate amplification of conditioned danger signals in human visual cortex. *Eur J Neurosci* 38: 3356–3362, 2013. doi:10.1111/ejn.12316.

Keitel C, Quigley C, Ruhnau P. Stimulus-driven brain oscillations in the alpha range: entrainment of intrinsic rhythms or frequency-following response? *J Neurosci* 34: 10137–10140, 2014. doi:10.1523/JNEUROSCI.1904-14.2014.

Keitel C, Thut G, Gross J. Visual cortex responses reflect temporal structure of continuous quasi-rhythmic sensory stimulation. *Neuroimage* 146: 58–70, 2017. doi:10.1016/j.neuroimage.2016.11.043.

Kim YJ, Grabowecky M, Paller KA, Muthu K, Suzuki S. Attention induces synchronization-based response gain in steady-state visual evoked potentials. *Nat Neurosci* 10: 117–125, 2007. doi:10.1038/nn1821.

Kim YJ, Grabowecky M, Paller KA, Suzuki S. Differential roles of frequency-following and frequency-doubling visual responses revealed by evoked neural harmonics. *J Cogn Neurosci* 23: 1875–1886, 2011. doi:10.1162/jocn.2010.21536.

Knill DC, Field D, Kersten D. Human discrimination of fractal images. *J Opt Soc Am A* 7: 1113–1123, 1990. doi:10.1364/JOSAA.7.001113.

Koenig-Robert R, VanRullen R. SWIFT: a novel method to track the neural correlates of recognition. *Neuroimage* 81: 273–282, 2013. doi:10.1016/j.neuroimage.2013.04.116.

Krolak-Salmon P, Hénaff MA, Tallon-Baudry C, Yvert B, Guénot M, Vighetto A, Mauguière F, Bertrand O. Human lateral geniculate nucleus and visual cortex respond to screen flicker. *Ann Neurol* 53: 73–80, 2003. doi:10.1002/ana.10403.

Lithari C, Sánchez-García C, Ruhnau P, Weisz N. Large-scale network-level processes during entrainment. *Brain Res* 1635: 143–152, 2016. doi:10.1016/j.brainres.2016.01.043.

Lopes da Silva FH, Harding GF. Transition to seizure in photosensitive epilepsy. *Epilepsy Res* 97: 278–282, 2011. doi:10.1016/j.eplepsyres.2011.10.022.

Martens U, Trujillo-Barreto N, Gruber T. Perceiving the tree in the woods: segregating brain responses to stimuli constituting natural scenes. *J Neurosci* 31: 17713–17718, 2011. doi:10.1523/JNEUROSCI.4743-11.2011.

Martens U, Wahl P, Hassler U, Friese U, Gruber T. Implicit and explicit contributions to object recognition: evidence from rapid perceptual learning. *PLoS One* 7: e47009, 2012. doi:10.1371/journal.pone.0047009.

McKeeff TJ, Remus DA, Tong F. Temporal limitations in object processing across the human ventral visual pathway. *J Neurophysiol* 98: 382–393, 2007. doi:10.1152/jn.00568.2006.

Miskovic V, Martinovic J, Wieser MJ, Petro NM, Bradley MM, Keil A. Electrocortical amplification for emotionally arousing natural scenes: the contribution of luminance and chromatic visual channels. *Biol Psychol* 106: 11–17, 2015. doi:10.1016/j.biopsycho.2015.01.012.

Moratti S, Clementz BA, Gao Y, Ortiz T, Keil A. Neural mechanisms of evoked oscillations: stability and interaction with transient events. *Hum Brain Mapp* 28: 1318–1333, 2007. doi:10.1002/hbm.20342.

Moratti S, Keil A. Not what you expect: experience but not expectancy predicts conditioned responses in human visual and supplementary cortex. *Cereb Cortex* 19: 2803–2809, 2009. doi:10.1093/cercor/bhp052.

Morey RD. Confidence intervals from normalized data: a correction to Cousineau (2005). *Tutor Quant Methods Psychol* 4: 61–64, 2008. doi:10.20982/tqmp.04.2.p061.

Morgan ST, Hansen JC, Hillyard SA. Selective attention to stimulus location modulates the steady-state visual evoked potential. *Proc Natl Acad Sci USA* 93: 4770–4774, 1996. doi:10.1073/pnas.93.10.4770.

Müller MM, Hübner R. Can the spotlight of attention be shaped like a doughnut? Evidence from steady-state visual evoked potentials. *Psychol Sci* 13: 119–124, 2002. doi:10.1111/1467-9280.00422.

Norcia AM, Appelbaum LG, Ales JM, Cottereau BR, Rossion B. The steady-state visual evoked potential in vision research: a review. *J Vis* 15: 1–46, 2015. doi:10.1167/15.6.4.

Olshausen BA, Field DJ. How close are we to understanding V1? *Neural Comput* 17: 1665–1699, 2005. doi:10.1162/0899766054026639.

Párraga CA, Troscianko T, Tolhurst DJ. The human visual system is optimised for processing the spatial information in natural visual images. *Curr Biol* 10: 35–38, 2000. doi:10.1016/S0960-9822(99)00262-6.

Pastor MA, Artieda J, Arbizu J, Valencia M, Masdeu JC. Human cerebral activation during steady-state visual-evoked responses. *J Neurosci* 23: 11621–11627, 2003.

Pastor MA, Valencia M, Artieda J, Alegre M, Masdeu JC. Topography of cortical activation differs for fundamental and harmonic frequencies of the steady-state visual-evoked responses. An EEG and PET H215O study. *Cereb Cortex* 17: 1899–1905, 2007. doi:10.1093/cercor/bhl098.

Perna A, Tosetti M, Montanaro D, Morrone MC. BOLD response to spatial phase congruency in human brain. *J Vis* 8: 1–15, 2008. doi:10.1167/8.10.15.

Peyk P, De Cesarei A, Junghöfer M. ElectroMagneticEncephalography software: overview and integration with other EEG/MEG toolboxes. *Comput Intell Neurosci* 2011: 861705, 2011. doi:10.1155/2011/861705.

Rager G, Singer W. The response of cat visual cortex to flicker stimuli of variable frequency. *Eur J Neurosci* 10: 1856–1877, 1998. doi:10.1046/j.1460-9568.1998.00197.x.

Regan D. *Human Brain Electrophysiology: Evoked Potentials and Evoked Magnetic Fields in Science and Medicine*. Norwalk, CT: Appleton and Lange, 1989.

Remole A. Luminance thresholds for subjective patterns in a flickering field: effect of wavelength. *J Opt Soc Am* 61: 1164–1168, 1971. doi:10.1364/JOSA.61.001164.

Retter TL, Rossion B. Uncovering the neural magnitude and spatio-temporal dynamics of natural image categorization in a fast visual stream. *Neuropsychologia* 91: 9–28, 2016. doi:10.1016/j.neuropsychologia.2016.07.028.

Roberts JA, Robinson PA. Quantitative theory of driven nonlinear brain dynamics. *Neuroimage* 62: 1947–1955, 2012. doi:10.1016/j.neuroimage.2012.05.054.

Rossion B. Understanding face perception by means of human electrophysiology. *Trends Cogn Sci* 18: 310–318, 2014. doi:10.1016/j.tics.2014.02.013.

Shapley R. Linear and nonlinear systems analysis of the visual system: why does it seem so linear? A review dedicated to the memory of Henk Spekreijse. *Vision Res* 49: 907–921, 2009. doi:10.1016/j.visres.2008.09.026.

Simoncelli EP, Olshausen BA. Natural image statistics and neural representation. *Annu Rev Neurosci* 24: 1193–1216, 2001. doi:10.1146/annurev.neuro.24.1.1193.

Singh KD, Smith AT, Greenlee MW. Spatiotemporal frequency and direction sensitivities of human visual areas measured using fMRI. *Neuroimage* 12: 550–564, 2000. doi:10.1006/nimg.2000.0642.

Spaak E, de Lange FP, Jensen O. Local entrainment of α oscillations by visual stimuli causes cyclic modulation of perception. *J Neurosci* 34: 3536–3544, 2014. doi:10.1523/JNEUROSCI.4385-13.2014.

Tadmor Y, Tolhurst DJ. Discrimination of changes in the second-order statistics of natural and synthetic images. *Vision Res* 34: 541–554, 1994. doi:10.1016/0042-6989(94)90167-8.

Tolhurst DJ, Tadmor Y, Chao T. Amplitude spectra of natural images. *Ophthalmic Physiol Opt* 12: 229–232, 1992. doi:10.1111/j.1475-1313.1992.tb00296.x.

Torralba A, Oliva A. Statistics of natural image categories. *Network* 14: 391–412, 2003. doi:10.1088/0954-898X_14_3_302.

Tyler CW, Apkarian P, Nakayama K. Multiple spatial-frequency tuning of electrical responses from human visual cortex. *Exp Brain Res* 33: 535–550, 1978. doi:10.1007/BF00235573.

van Hateren JH, van der Schaaf A. Independent component filters of natural images compared with simple cells in primary visual cortex. *Proc Biol Sci* 265: 359–366, 1998. doi:10.1098/rspb.1998.0303.

Vialatte FB, Maurice M, Dauwels J, Cichocki A. Steady-state visually evoked potentials: focus on essential paradigms and future perspectives. *Prog Neurobiol* 90: 418–438, 2010. doi:10.1016/j.pneurobio.2009.11.005.

Wieser MJ, Miskovic V, Keil A. Steady-state visual evoked potentials as a research tool in social affective neuroscience. *Psychophysiology* 53: 1763–1775, 2016. doi:10.1111/psyp.12768.

Williams PE, Mechler F, Gordon J, Shapley R, Hawken MJ. Entrainment to video displays in primary visual cortex of macaque and humans. *J Neurosci* 24: 8278–8288, 2004. doi:10.1523/JNEUROSCI.2716-04.2004.

Yeatman JD, Norcia AM. Temporal tuning of word- and face-selective cortex. *J Cogn Neurosci* 28: 1820–1827, 2016. doi:10.1162/jocn_a_01002.